# Searching for Dark Matter Annihilation from Milky Way Dwarf Spheroidal Galaxies with Six Years of Fermi Large Area Telescope Data

M. Ackermann,[1] A. Albert,[2] B. Anderson,[3,4,*] W. B. Atwood,[5] L. Baldini,[6,2] G. Barbiellini,[7,8] D. Bastieri,[9,10] K. Bechtol,[11] R. Bellazzini,[12] E. Bissaldi,[13] R. D. Blandford,[2] E. D. Bloom,[2] R. Bonino,[14,15] E. Bottacini,[2] T. J. Brandt,[16] J. Bregeon,[17] P. Bruel,[18] R. Buehler,[1] G. A. Caliandro,[2,19] R. A. Cameron,[2] R. Caputo,[5] M. Caragiulo,[13] P. A. Caraveo,[20] C. Cecchi,[21,22] E. Charles,[2] A. Chekhtman,[23,§] J. Chiang,[2] G. Chiaro,[10] S. Ciprini,[24,21,25] R. Claus,[2] J. Cohen-Tanugi,[17] J. Conrad,[3,4,26] A. Cuoco,[14,15] S. Cutini,[24,25,21] F. D'Ammando,[27,28] A. de Angelis,[29] F. de Palma,[13,30] R. Desiante,[31,14] S. W. Digel,[2] L. Di Venere,[32] P. S. Drell,[2] A. Drlica-Wagner,[33,†] R. Essig,[34] C. Favuzzi,[32,13] S. J. Fegan,[18] E. C. Ferrara,[16] W. B. Focke,[2] A. Franckowiak,[2] Y. Fukazawa,[35] S. Funk,[36] P. Fusco,[32,13] F. Gargano,[13] D. Gasparrini,[24,25,21] N. Giglietto,[32,13] F. Giordano,[32,13] M. Giroletti,[27] T. Glanzman,[2] G. Godfrey,[2] G. A. Gomez-Vargas,[37,38] I. A. Grenier,[39] S. Guiriec,[16,40] M. Gustafsson,[41] E. Hays,[16] J. W. Hewitt,[42] D. Horan,[18] T. Jogler,[2] G. Jóhannesson,[43] M. Kuss,[12] S. Larsson,[44,4] L. Latronico,[14] J. Li,[45] L. Li,[44,4] M. Llena Garde,[3,4] F. Longo,[7,8] F. Loparco,[32,13] P. Lubrano,[21,22] D. Malyshev,[2] M. Mayer,[1] M. N. Mazziotta,[13] J. E. McEnery,[16,46] M. Meyer,[3,4] P. F. Michelson,[2] T. Mizuno,[47] A. A. Moiseev,[48,46] M. E. Monzani,[2] A. Morselli,[37] S. Murgia,[49] E. Nuss,[17] T. Ohsugi,[47] M. Orienti,[27] E. Orlando,[2] J. F. Ormes,[50] D. Paneque,[51,2] J. S. Perkins,[16] M. Pesce-Rollins,[12,2] F. Piron,[17] G. Pivato,[12] T. A. Porter,[2] S. Rainò,[32,13] R. Rando,[9,10] M. Razzano,[12] A. Reimer,[52,2] O. Reimer,[52,2] S. Ritz,[5] M. Sánchez-Conde,[4,3] A. Schulz,[1] N. Sehgal,[53] C. Sgrò,[12] E. J. Siskind,[54] F. Spada,[12] G. Spandre,[12] P. Spinelli,[32,13] L. Strigari,[55] H. Tajima,[56,2] H. Takahashi,[35] J. B. Thayer,[2] L. Tibaldo,[2] D. F. Torres,[45,57] E. Troja,[16,46] G. Vianello,[2] M. Werner,[52] B. L. Winer,[58] K. S. Wood,[59] M. Wood,[2,‡] G. Zaharijas,[60,61] and S. Zimmer[3,4]

(The Fermi-LAT Collaboration)

[1]*Deutsches Elektronen Synchrotron DESY, D-15738 Zeuthen, Germany*
[2]*W. W. Hansen Experimental Physics Laboratory, Kavli Institute for Particle Astrophysics and Cosmology, Department of Physics and SLAC National Accelerator Laboratory, Stanford University, Stanford, California 94305, USA*
[3]*Department of Physics, Stockholm University, AlbaNova, SE-106 91 Stockholm, Sweden*
[4]*The Oskar Klein Centre for Cosmoparticle Physics, AlbaNova, SE-106 91 Stockholm, Sweden*
[5]*Santa Cruz Institute for Particle Physics, Department of Physics and Department of Astronomy and Astrophysics, University of California at Santa Cruz, Santa Cruz, California 95064, USA*
[6]*Università di Pisa and Istituto Nazionale di Fisica Nucleare, Sezione di Pisa I-56127 Pisa, Italy*
[7]*Istituto Nazionale di Fisica Nucleare, Sezione di Trieste, I-34127 Trieste, Italy*
[8]*Dipartimento di Fisica, Università di Trieste, I-34127 Trieste, Italy*
[9]*Istituto Nazionale di Fisica Nucleare, Sezione di Padova, I-35131 Padova, Italy*
[10]*Dipartimento di Fisica e Astronomia "G. Galilei", Università di Padova, I-35131 Padova, Italy*
[11]*Dept. of Physics and Wisconsin IceCube Particle Astrophysics Center, University of Wisconsin, Madison, Wisconsin 53706, USA*
[12]*Istituto Nazionale di Fisica Nucleare, Sezione di Pisa, I-56127 Pisa, Italy*
[13]*Istituto Nazionale di Fisica Nucleare, Sezione di Bari, I-70126 Bari, Italy*
[14]*Istituto Nazionale di Fisica Nucleare, Sezione di Torino, I-10125 Torino, Italy*
[15]*Dipartimento di Fisica Generale "Amadeo Avogadro", Università degli Studi di Torino, I-10125 Torino, Italy*
[16]*NASA Goddard Space Flight Center, Greenbelt, Maryland 20771, USA*
[17]*Laboratoire Univers et Particules de Montpellier, Université Montpellier, CNRS/IN2P3, Montpellier, France*
[18]*Laboratoire Leprince-Ringuet, École polytechnique, CNRS/IN2P3, Palaiseau, France*
[19]*Consorzio Interuniversitario per la Fisica Spaziale (CIFS), I-10133 Torino, Italy*
[20]*INAF-Istituto di Astrofisica Spaziale e Fisica Cosmica, I-20133 Milano, Italy*
[21]*Istituto Nazionale di Fisica Nucleare, Sezione di Perugia, I-06123 Perugia, Italy*
[22]*Dipartimento di Fisica, Università degli Studi di Perugia, I-06123 Perugia, Italy*
[23]*College of Science, George Mason University, Fairfax, Virginia 22030, USA*
[24]*Agenzia Spaziale Italiana (ASI) Science Data Center, I-00133 Roma, Italy*
[25]*INAF Osservatorio Astronomico di Roma, I-00040 Monte Porzio Catone (Roma), Italy*
[26]*Wallenberg Academy Fellow*
[27]*INAF Istituto di Radioastronomia, I-40129 Bologna, Italy*
[28]*Dipartimento di Astronomia, Università di Bologna, I-40127 Bologna, Italy*
[29]*Dipartimento di Fisica, Università di Udine and Istituto Nazionale di Fisica Nucleare, Sezione di Trieste, Gruppo Collegato di Udine, I-33100 Udine*
[30]*Università Telematica Pegaso, Piazza Trieste e Trento, 48, I-80132 Napoli, Italy*

 

[31]Università di Udine, I-33100 Udine, Italy
[32]Dipartimento di Fisica "M. Merlin" dell'Università e del Politecnico di Bari, I-70126 Bari, Italy
[33]Center for Particle Astrophysics, Fermi National Accelerator Laboratory, Batavia, Illinois 60510, USA
[34]C.N. Yang Institute for Theoretical Physics, State University of New York, Stony Brook, New York 11794-3840, USA
[35]Department of Physical Sciences, Hiroshima University, Higashi-Hiroshima, Hiroshima 739-8526, Japan
[36]Erlangen Centre for Astroparticle Physics, D-91058 Erlangen, Germany
[37]Istituto Nazionale di Fisica Nucleare, Sezione di Roma "Tor Vergata", I-00133 Roma, Italy
[38]Departamento de Fisíca, Pontificia Universidad Católica de Chile, Avenida Vicuña Mackenna 4860, Santiago, Chile
[39]Laboratoire AIM, CEA-IRFU/CNRS/Université Paris Diderot, Service d'Astrophysique, CEA Saclay, F-91191 Gif sur Yvette, France
[40]NASA Postdoctoral Program Fellow, USA
[41]Georg-August University Göttingen, Institute for theoretical Physics—Faculty of Physics, Friedrich-Hund-Platz 1, D-37077 Göttingen, Germany
[42]University of North Florida, Department of Physics, 1 UNF Drive, Jacksonville, Florida 32224, USA
[43]Science Institute, University of Iceland, IS-107 Reykjavik, Iceland
[44]Department of Physics, KTH Royal Institute of Technology, AlbaNova, SE-106 91 Stockholm, Sweden
[45]Institute of Space Sciences (IEEC-CSIC), Campus UAB, E-08193 Barcelona, Spain
[46]Department of Physics and Department of Astronomy, University of Maryland, College Park, Maryland 20742, USA
[47]Hiroshima Astrophysical Science Center, Hiroshima University, Higashi-Hiroshima, Hiroshima 739-8526, Japan
[48]Center for Research and Exploration in Space Science and Technology (CRESST) and NASA Goddard Space Flight Center, Greenbelt, Maryland 20771, USA
[49]Center for Cosmology, Physics and Astronomy Department, University of California, Irvine, California 92697-2575, USA
[50]Department of Physics and Astronomy, University of Denver, Denver, CO 80208, USA
[51]Max-Planck-Institut für Physik, D-80805 München, Germany
[52]Institut für Astro- und Teilchenphysik and Institut für Theoretische Physik, Leopold-Franzens-Universität Innsbruck, A-6020 Innsbruck, Austria
[53]Physics and Astronomy Department, Stony Brook University, Stony Brook, New York 11794, USA
[54]NYCB Real-Time Computing Inc., Lattingtown, New York 11560-1025, USA
[55]Texas A&M University, Department of Physics and Astronomy, College Station, Texas 77843-4242, USA
[56]Solar-Terrestrial Environment Laboratory, Nagoya University, Nagoya 464-8601, Japan
[57]Institució Catalana de Recerca i Estudis Avançats (ICREA), Barcelona, Spain
[58]Department of Physics, Center for Cosmology and Astro-Particle Physics, The Ohio State University, Columbus, Ohio 43210, USA
[59]Space Science Division, Naval Research Laboratory, Washington, DC 20375-5352, USA
[60]Istituto Nazionale di Fisica Nucleare, Sezione di Trieste, and Università di Trieste, I-34127 Trieste, Italy
[61]Laboratory for Astroparticle Physics, University of Nova Gorica, Vipavska 13, SI-5000 Nova Gorica, Slovenia

(Received 10 March 2015; revised manuscript received 15 July 2015; published 30 November 2015)

The dwarf spheroidal satellite galaxies (dSphs) of the Milky Way are some of the most dark matter (DM) dominated objects known. We report on $\gamma$-ray observations of Milky Way dSphs based on six years of Fermi Large Area Telescope data processed with the new Pass8 event-level analysis. None of the dSphs are significantly detected in $\gamma$ rays, and we present upper limits on the DM annihilation cross section from a combined analysis of 15 dSphs. These constraints are among the strongest and most robust to date and lie below the canonical thermal relic cross section for DM of mass $\lesssim$100 GeV annihilating via quark and $\tau$-lepton channels.

DOI: 10.1103/PhysRevLett.115.231301 95.35.+d, 95.85.Pw, 98.56.Wm, 98.70.Rz

*Introduction.*—Approximately 26% of the energy density of the Universe is composed of nonbaryonic cold dark matter (DM) [1]. Weakly interacting massive particles (WIMPs) are an attractive candidate to constitute some or all of DM [2–4]. The relic abundance of WIMPs is determined by their annihilation cross section at freeze-out [5], and the characteristic weak-scale cross sections of WIMPs can naturally produce a relic abundance equal to the observed abundance of DM. Self-annihilation of WIMPs would continue today in regions of high DM density and result in the production of energetic standard model particles. The large mass of the WIMP ($m_{\rm DM}$) permits the production of $\gamma$ rays observable by the Fermi Large Area Telescope (LAT), which is sensitive to energies ranging from 20 MeV to >300 GeV.

Kinematic data indicate that the dwarf spheroidal satellite galaxies (dSphs) of the Milky Way contain a substantial DM component [6,7]. The $\gamma$-ray signal flux at the LAT, $\phi_s$ (ph cm$^{-2}$ s$^{-1}$), expected from the annihilation of DM with a density distribution $\rho_{\rm DM}(\boldsymbol{r})$ is given by

$$\phi_s(\Delta\Omega) = \underbrace{\frac{1}{4\pi}\frac{\langle\sigma v\rangle}{2m_{\rm DM}^2}\int_{E_{\rm min}}^{E_{\rm max}}\frac{dN_\gamma}{dE_\gamma}dE_\gamma}_{\text{particle physics}} \times \underbrace{\int_{\Delta\Omega}\int_{\rm LOS}\rho_{\rm DM}^2(\boldsymbol{r})dld\Omega'}_{J\text{ factor}}. \quad (1)$$

Here, the first term is dependent on the particle physics properties—i.e., the thermally averaged annihilation cross section $\langle\sigma v\rangle$, the particle mass $m_{\rm DM}$, and the differential $\gamma$-ray yield per annihilation $dN_\gamma/dE_\gamma$, integrated over the experimental energy range. [Strictly speaking, the differential yield per annihilation in Eq. (1) is a sum of differential yields into specific final states: $dN_\gamma/dE_\gamma = \sum_f B_f dN_\gamma^f/dE_\gamma$, where $B_f$ is the branching fraction into final state $f$. Here, we make use of Eq. (1) in the context of single final states only.] The second term, known as the $J$ factor, is the line-of-sight (LOS) integral through the DM distribution integrated over a solid angle $\Delta\Omega$.

Milky Way dSphs can give rise to $J$ factors in excess of $10^{19}$ GeV$^2$ cm$^{-5}$ [8,9], which, coupled with their lack of nonthermal astrophysical processes, makes them good targets for DM searches via $\gamma$ rays. $\gamma$-ray searches for dSphs yield some of the most stringent constraints on $\langle\sigma v\rangle$, particularly when multiple dSphs are analyzed together using a joint likelihood technique [10–15]. Limits on $\langle\sigma v\rangle$ derived from observations of dSphs have begun to probe the low-$m_{\rm DM}$ parameter space for which the WIMP abundance matches the observed DM relic density.

In contrast, DM searches in the Galactic center take advantage of a $J$ factor that is $O(100)$ times larger, although $\gamma$-ray emission from nonthermal processes makes a bright, structured background. Several studies of the Galactic center interpret an excess of $\gamma$ rays with respect to modeled astrophysical backgrounds as a signal of 20–50 GeV WIMPs annihilating via the $b\bar{b}$ channel [16–19]. Coincidentally, the largest deviation from expected background in some previous studies of dSphs occurred for a similar set of WIMP characteristics; however, this deviation was not statistically significant [13].

Using a new LAT event-level analysis, known as PASS8, we reexamine the sample of 25 Milky Way dSphs from Ackermann *et al.* [13] using six years of LAT data. The PASS8 data benefit from an improved point-spread function (PSF), effective area, and energy reach. More accurate Monte Carlo simulations of the detector and the environment in low-Earth orbit have reduced the systematic uncertainty in the LAT instrument response functions (IRFs) [20]. Within the standard photon classes, PASS8 offers event types, subdivisions based on event-by-event uncertainties in the directional and energy measurements, which can increase the sensitivity of likelihood-based analyses. In this work we use a set of four PSF event-type selections that subdivide the events in our data sample according to the quality of their directional reconstruction. In addition to the improvements from PASS8, we employ the updated third LAT source catalog (3FGL), based on four years of PASS7 REPROCESSED data, to model pointlike background sources [21]. Together, these improvements, along with an additional two years of data taking, lead to a predicted increase in sensitivity of 70% relative to the four-year analysis of Ackermann *et al.* [13] for the $b\bar{b}$ channel at 100 GeV. More details on PASS8 and other aspects of this analysis can be found in the Supplemental Material [22].

*LAT data selection.*—We examine six years of LAT data (August 4, 2008 to August 5, 2014) selecting PASS8 SOURCE-class events in the energy range between 500 MeV and 500 GeV. We select the 500 MeV lower limit to mitigate the impact of leakage from the bright limb of the Earth because the PSF broadens considerably below that energy. To further avoid contamination from terrestrial $\gamma$ rays, events with zenith angles larger than 100° are rejected. We also remove time intervals around bright gamma-ray bursts (GRBs) and solar flares following the prescription used for the 3FGL catalog. We extract from this data set $10^\circ \times 10^\circ$ square regions of interest (ROIs) in Galactic coordinates centered at the position of each dSph specified in Table I.

At a given energy, 20%–40% of the events classified as photons in our six-year PASS8 data set are shared with the analysis of Ackermann *et al.* [13]. The low fraction of shared events can be attributed primarily to the larger time range used for the present analysis (four versus six years) and the increase in $\gamma$-ray acceptance of the P8R2_SOURCE event class relative to P7REP_CLEAN. At most, the PASS7 events can represent 35%–50% of the new, larger sample. Migration of the individual reconstructed events, particularly residual cosmic rays, across ROI and class selection boundaries further reduces the overlap, making the two analyses nearly statistically independent [22].

*J factors for dwarf spheroidal galaxies.*—The DM content of dSphs can be determined through dynamical modeling of their stellar density and velocity dispersion profiles [42–44]. Recent studies have shown that an accurate estimate of the dynamical mass of a dSph can be derived from measurements of the average stellar velocity dispersion and half-light radius alone [45,46]. The total mass within the half-light radius and the integrated $J$ factor have been found to be fairly insensitive to the assumed DM density profile [13,44,47]. We assume that the DM distribution in dSphs follows a Navarro-Frenk-White (NFW) profile [48]

$$\rho_{\rm DM}(r) = \frac{\rho_0 r_s^3}{r(r_s + r)^2}, \quad (2)$$

where $r_s$ and $\rho_0$ are the NFW scale radius and characteristic density, respectively. We take $J$ factors and other physical

TABLE I. Properties of Milky Way dSphs.

| Name | $\ell$[a] (deg) | $b$[a] (deg) | Distance (kpc) | $\log_{10}(J_{\rm obs})$[b] ($\log_{10}$[GeV$^2$ cm$^{-5}$]) | Ref. |
|---|---|---|---|---|---|
| Bootes I | 358.1 | 69.6 | 66 | $18.8 \pm 0.22$ | [34] |
| Canes Venatici II | 113.6 | 82.7 | 160 | $17.9 \pm 0.25$ | [35] |
| Carina | 260.1 | −22.2 | 105 | $18.1 \pm 0.23$ | [36] |
| Coma Berenices | 241.9 | 83.6 | 44 | $19.0 \pm 0.25$ | [35] |
| Draco | 86.4 | 34.7 | 76 | $18.8 \pm 0.16$ | [37] |
| Fornax | 237.1 | −65.7 | 147 | $18.2 \pm 0.21$ | [36] |
| Hercules | 28.7 | 36.9 | 132 | $18.1 \pm 0.25$ | [35] |
| Leo II | 220.2 | 67.2 | 233 | $17.6 \pm 0.18$ | [38] |
| Leo IV | 265.4 | 56.5 | 154 | $17.9 \pm 0.28$ | [35] |
| Sculptor | 287.5 | −83.2 | 86 | $18.6 \pm 0.18$ | [36] |
| Segue 1 | 220.5 | 50.4 | 23 | $19.5 \pm 0.29$ | [39] |
| Sextans | 243.5 | 42.3 | 86 | $18.4 \pm 0.27$ | [36] |
| Ursa Major II | 152.5 | 37.4 | 32 | $19.3 \pm 0.28$ | [35] |
| Ursa Minor | 105.0 | 44.8 | 76 | $18.8 \pm 0.19$ | [37] |
| Willman 1 | 158.6 | 56.8 | 38 | $19.1 \pm 0.31$ | [40] |
| Bootes II[c] | 353.7 | 68.9 | 42 | – | – |
| Bootes III | 35.4 | 75.4 | 47 | – | – |
| Canes Venatici I | 74.3 | 79.8 | 218 | $17.7 \pm 0.26$ | [35] |
| Canis Major | 240.0 | −8.0 | 7 | – | – |
| Leo I | 226.0 | 49.1 | 254 | $17.7 \pm 0.18$ | [41] |
| Leo V | 261.9 | 58.5 | 178 | – | – |
| Pisces II | 79.2 | −47.1 | 182 | – | – |
| Sagittarius | 5.6 | −14.2 | 26 | – | – |
| Segue 2 | 149.4 | −38.1 | 35 | – | – |
| Ursa Major I | 159.4 | 54.4 | 97 | $18.3 \pm 0.24$ | [35] |

[a]Galactic longitude and latitude.
[b]$J$ factors are calculated assuming a NFW density profile and integrated over a circular region with a solid angle of $\Delta\Omega \sim 2.4 \times 10^{-4}$ sr (angular radius of 0.5°).
[c]dSphs below the horizontal line are not included in the combined analysis.

properties for the Milky Way dSphs from Ackermann *et al.* [13] (and references therein).

*Data analysis.*—We perform a binned Poisson maximum-likelihood analysis in 24 bins of energy (constraints are insensitive to finer binning), logarithmically spaced from 500 MeV to 500 GeV, and an 0.1° angular pixelization. The low-energy bound of 500 MeV is selected to mitigate the impact of leakage from the bright limb of the Earth, while the high-energy bound of 500 GeV is chosen to mitigate the effect of the increasing residual charged-particle background at higher energies [49]. The data were analyzed with the Fermi Science Tools [50] version 10-01-01 and the P8R2_SOURCE_V6 IRFs. Our diffuse background model includes a structured Galactic component and a spatially isotropic component that represents both extragalactic emission and residual particle contamination [51]. Because the energy resolution of the LAT was not accounted for when fitting the Galactic diffuse model, differences in response (energy resolution and effective area) between IRF sets lead to different measured intensities for this component. Thus, a small energy-dependent scaling has been applied to the PASS7 REPROCESSED Galactic diffuse model. Changes with respect to the PASS7 REPROCESSED model are less than 5% above 100 MeV. Details on the derivation of the rescaled model are given in Ref. [22]. The $\gamma$-ray characteristics of nearby pointlike sources are taken from the 3FGL catalog [21].

We perform a bin-by-bin likelihood analysis of the $\gamma$-ray emission coincident with each dSph following the procedure of Ackermann *et al.* [13]. The flux normalizations of the Galactic diffuse and isotropic components and 3FGL catalog sources within the $10° \times 10°$ ROI were fit simultaneously in a binned likelihood analysis over the broadband energy range from 500 MeV to 500 GeV. The normalizations of the background sources are insensitive to the inclusion of a putative power-law source at the locations of the dSphs, which is consistent with the lack of any strong signal associated with the dSphs. Fixing the normalizations of the background sources with the broadband fit before fitting each bin individually avoids numerical instability resulting from the fine binning in energy and the degeneracy of the diffuse background components at high Galactic latitudes.

After fixing the background normalizations, we scan the likelihood as a function of the flux normalization of the putative DM signal independently in each energy bin (this procedure is similar to that used to evaluate the spectral energy distribution of a source). Within each bin, we model

the putative dSph source with a power-law spectral model ($dN/dE \propto E^{-\Gamma}$) with spectral index of $\Gamma = 2$. By analyzing each energy bin separately, we avoid selecting a single spectral shape to span the entire energy range at the expense of introducing additional degrees of freedom into the fit.

While the bin-by-bin likelihood function is essentially independent of spectral assumptions, it does depend on the spatial model of the DM distribution in the dSphs. We model the dSphs with spatially extended NFW DM density profiles projected along the line of sight. The angular extent of the emission profile for each dSph is set by the scale radius of its DM halo, which contains approximately 90% of the total annihilation flux. We use the set of DM halo scale radii from Ackermann *et al.* [13], which span a range of subtended angles between 0.1° and 0.4°.

We test a wide range of DM annihilation hypotheses by using predicted $\gamma$-ray spectra to tie the signal normalization across the energy bins. Spectra for DM annihilation are generated with the DMFIT package based on PYTHIA 8.165 [13,52,53]. We reconstruct a broadband likelihood function by multiplying the bin-by-bin likelihood functions evaluated at the predicted fluxes for a given DM model.

We combine the broadband likelihood functions across 15 of the observed dSphs [54] and include statistical uncertainties on the $J$ factors of each dSph by adding an additional $J$ factor likelihood term to the binned Poisson likelihood for the LAT data. The $J$ factor likelihood for target $i$ is given by

$$\mathcal{L}_J(J_i|J_{\mathrm{obs,i}},\sigma_i) = \frac{1}{\ln(10)J_{\mathrm{obs,i}}\sqrt{2\pi}\sigma_i} \times e^{-[\log_{10}(J_i)-\log_{10}(J_{\mathrm{obs,i}})]^2/2\sigma_i^2}, \quad (3)$$

where $J_i$ is the true value of the $J$ factor and $J_{\mathrm{obs,i}}$ is the measured $J$ factor with error $\sigma_i$. This parametrization of the $J$ factor likelihood is obtained by fitting a log-normal function with peak value $J_{\mathrm{obs,i}}$ to the posterior distribution for each $J$ factor as derived by Martinez [8], providing a reasonable way to quantify the uncertainties on the $J$ factors. This approach is a slight modification of the approach in Ackermann *et al.* [10,13], where an effective likelihood was derived considering a flat prior on the $J$ factors. We note that the $J$ factor correction is only intended to incorporate the statistical uncertainty in the $J$ factors, and not the systematic uncertainty resulting from the fitting procedure or choice of priors [22]. More details on the derivation of the $J$ factor likelihood and the effects of systematic uncertainties can be found in the Supplemental Material [22].

Combining the broadband $\gamma$-ray and $J$ factor likelihood functions, our likelihood function for target $i$ becomes

$$\tilde{\mathcal{L}}_i(\boldsymbol{\mu},\boldsymbol{\theta}_i = \{\boldsymbol{\alpha}_i, J_i\}|\mathcal{D}_i) = \mathcal{L}_i(\boldsymbol{\mu},\boldsymbol{\theta}_i|\mathcal{D}_i)\mathcal{L}_J(J_i|J_{\mathrm{obs,i}},\sigma_i). \quad (4)$$

Here, $\boldsymbol{\mu}$ are the parameters of the DM model, $\boldsymbol{\theta}_i$ is the set of nuisance parameters that includes both nuisance parameters from the LAT analysis ($\alpha_i$) and the dSph $J$ factor ($J_i$), and $\mathcal{D}_i$ represents the $\gamma$-ray data. We incorporate additional information about the event-wise quality of the angular reconstruction by forming the LAT likelihood function ($\mathcal{L}_i$) from the product of likelihood functions for four PSF event types. The four PSF event types (PSF0, PSF1, PSF2, and PSF3) subdivide the events in the SOURCE-class data set into exclusive partitions ($\mathcal{D}_{i,j}$) in order of decreasing uncertainty on the direction measurement. The resulting joint LAT likelihood function is given by

$$\mathcal{L}_i(\boldsymbol{\mu},\boldsymbol{\theta}_i|\mathcal{D}_i) = \prod_j \mathcal{L}_i(\boldsymbol{\mu},\boldsymbol{\theta}_i|\mathcal{D}_{i,j}). \quad (5)$$

The spectral and spatial model of $\gamma$-ray counts for each event-type partition is evaluated using a set of IRFs computed for that class and type selection.

We evaluate the significance of DM hypotheses using a test statistic (TS) defined as

$$\mathrm{TS} = -2\ln\left(\frac{\mathcal{L}(\boldsymbol{\mu}_0,\hat{\boldsymbol{\theta}}|\mathcal{D})}{\mathcal{L}(\hat{\boldsymbol{\mu}},\hat{\boldsymbol{\theta}}|\mathcal{D})}\right), \quad (6)$$

where $\boldsymbol{\mu}_0$ are the parameters of the null (no DM) hypothesis and $\hat{\boldsymbol{\mu}}$ and $\hat{\boldsymbol{\theta}}$ are the best-fit parameters under the DM hypothesis. $\mathcal{L}$ can here be either the likelihood for an individual dSph or the joint likelihood for the dSphs in our combined sample. We note that following the methodology of Ackermann *et al.* [13] we use background parameters ($\hat{\boldsymbol{\theta}}$) derived under the hypothesis of a DM source with a $\Gamma = 2$ power-law spectrum when evaluating both the null and DM hypotheses. This is a good approximation as long as the best-fit signal is small relative to the background in the ROI. Based on the asymptotic theorem of Chernoff [55], the TS can be converted to a significance based on a mixture of $\chi^2$ distributions. The validity of this assumption is examined further in the Supplemental Material [22].

*Results.*—We find no significant $\gamma$-ray excess associated with the Milky Way dSphs when analyzed individually or as a population. In the combined analysis of 15 dSphs, the largest deviation from the background-only hypothesis has $\mathrm{TS} = 1.3$ occurring for $m_{\mathrm{DM}} = 2$ GeV annihilating through the $e^+e^-$ channel. Among the dSphs in our combined analysis, the dSph with the largest individual significance is Sculptor with $\mathrm{TS} = 4.3$ for $m_{\mathrm{DM}} = 5$ GeV annihilating through the $\mu^+\mu^-$ channel. The maximum TS of our combined analysis is well below the threshold set for $\gamma$-ray source detection and is completely consistent with a background fluctuation [21]. We set upper limits on $\langle\sigma v\rangle$ at the 95% confidence level (CL) for WIMPs with $m_{\mathrm{DM}}$ between 2 GeV and 10 TeV annihilating into six different standard model channels ($b\bar{b}$, $\tau^+\tau^-$, $\mu^+\mu^-$, $e^+e^-$, $W^+W^-$, $u\bar{u}$) [56]. Figure 1 shows the comparison of the limits for

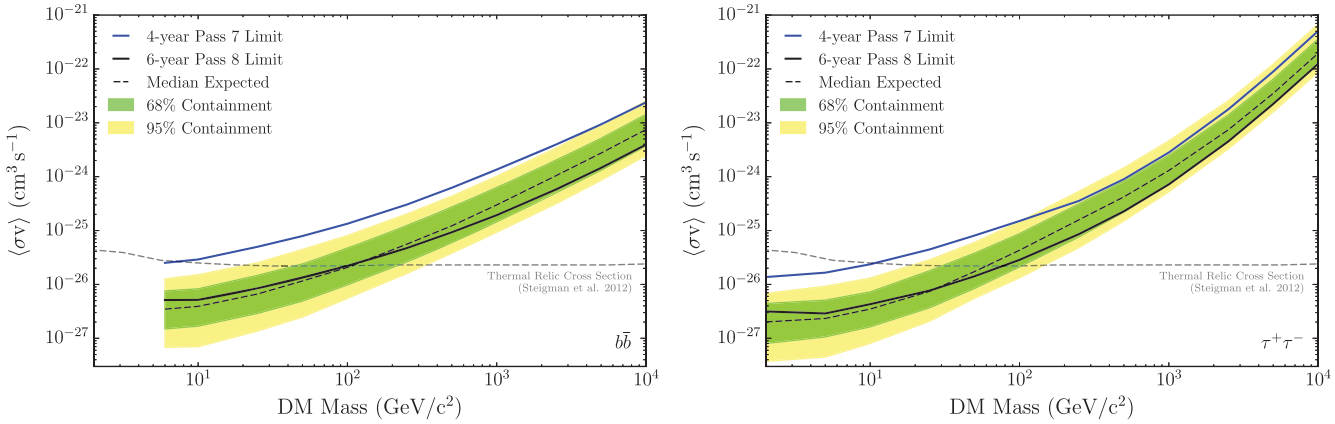


FIG. 1 (color). Constraints on the DM annihilation cross section at the 95% CL for the $b\bar{b}$ (left) and $\tau^+\tau^-$ (right) channels derived from a combined analysis of 15 dSphs. Bands for the expected sensitivity are calculated by repeating the same analysis on 300 randomly selected sets of high-Galactic-latitude blank fields in the LAT data. The dashed line shows the median expected sensitivity while the bands represent the 68% and 95% quantiles. For each set of random locations, nominal $J$ factors are randomized in accord with their measurement uncertainties. The solid blue curve shows the limits derived from a previous analysis of four years of PASS7 REPROCESSED data and the same sample of 15 dSphs [13]. The dashed gray curve in this and subsequent figures corresponds to the thermal relic cross section from Steigman *et al.* [5].

the $b\bar{b}$ and $\tau^+\tau^-$ channels with expectation bands derived from the analysis of 300 randomly selected sets of blank fields. Sets of blank fields are generated by choosing random sky positions with $|b| > 30°$ that are centered at least 0.5° from 3FGL catalog sources. We additionally require fields within each set to be separated by at least 7°. Our expected limit bands are evaluated with the 3FGL source catalog based on four years of PASS7 REPROCESSED data and account for the influence of new sources present in the six-year PASS8 data set.

Comparing with the results of Ackermann *et al.* [13], we find a factor of 3–5 improvement in the limits for all channels using six years of PASS8 data and the same sample of 15 dSphs. The larger data set as well as the gains in the LAT instrument performance enabled by PASS8 both contribute to the increased sensitivity of the present analysis. An additional 30%–40% improvement in the limit can be attributed to the modified functional form chosen for the $J$ factor likelihood (3). Statistical fluctuations in the PASS8 data set also play a substantial role. Because the PASS8 six-year and PASS7 REPROCESSED four-year event samples have a shared fraction of only 20%–40%, the two analyses are nearly statistically independent. For masses below 100 GeV, the upper limits of Ackermann *et al.* [13] were near the 95% upper bound of the expected sensitivity band while the limits in the present analysis are within 1 standard deviation of the median expectation value.

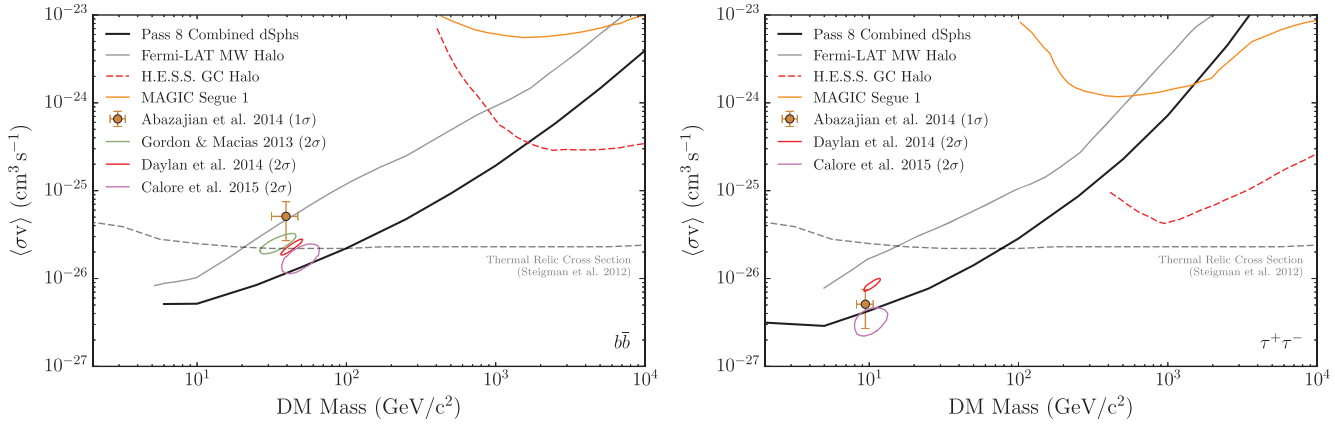


FIG. 2 (color). Comparison of constraints on the DM annihilation cross section for the $b\bar{b}$ (left) and $\tau^+\tau^-$ (right) channels from this work with previously published constraints from LAT analysis of the Milky Way halo ($3\sigma$ limit) [57], 112 hours of observations of the Galactic center with H.E.S.S. [58], and 157.9 hours of observations of Segue 1 with MAGIC [59]. Pure annihilation channel limits for the Galactic center H.E.S.S. observations are taken from Abazajian and Harding [60] and assume an Einasto Milky Way density profile with $\rho_\odot = 0.389$ GeV cm$^{-3}$. Closed contours and the marker with error bars show the best-fit cross section and mass from several interpretations of the Galactic center excess [16–19].

Uncertainties in the LAT IRFs, modeling of the diffuse background, and estimation of $J$ factors all contribute systematic errors to this analysis. By examining maximal variations of each contributor, we find that at 100 GeV they lead to $\pm 9\%$, $\pm 8\%$, and $\pm 33\%$ shifts in our limits, respectively (see the Supplemental Material [22]).

Our results begin to constrain some of the preferred parameter space for a DM interpretation of a $\gamma$-ray excess in the Galactic center region [16–19]. As shown in Fig. 2, for interpretations assuming a $b\bar{b}$ final state, the best-fit models lie in a region of parameter space slightly above the 95% CL upper limit from this analysis, with an annihilation cross section in the range of $(1\text{–}3) \times 10^{-26}$ cm$^3$ s$^{-1}$ and $m_{\rm DM}$ between 25 and 50 GeV. However, uncertainties in the structure of the Galactic DM distribution and the Galactic diffuse backgrounds can significantly enlarge the best-fit regions of $\langle \sigma v \rangle$, channel, and $m_{\rm DM}$ [61].

In conclusion, we present a combined analysis of 15 Milky Way dSphs using a new and improved LAT data set processed with the Pass8 event-level analysis. We exclude the thermal relic annihilation cross section ($\sim 2.2 \times 10^{-26}$ cm$^3$ s$^{-1}$) for WIMPs with $m_{\rm DM} \lesssim 100$ GeV annihilating through the quark and $\tau$-lepton channels. Our results also constrain DM particles with $m_{\rm DM}$ above 100 GeV surpassing the best limits from imaging atmospheric Cherenkov telescopes for masses up to $\sim$1 TeV for quark channels and $\sim$300 GeV for the $\tau$-lepton channel. These constraints include the statistical uncertainty on the DM content of the dSphs. The future sensitivity to DM annihilation in dSphs will benefit from additional LAT data taking and the discovery of new dSphs with upcoming optical surveys such as the Dark Energy Survey [62] and the Large Synoptic Survey Telescope [63].

The Fermi-LAT Collaboration acknowledges support for LAT development, operation, and data analysis from NASA and DOE (United States), CEA/Irfu and IN2P3/CNRS (France), ASI and INFN (Italy), MEXT, KEK, and JAXA (Japan), and the K. A. Wallenberg Foundation, the Swedish Research Council, and the National Space Board (Sweden). Science analysis support in the operations phase from INAF (Italy) and CNES (France) is also gratefully acknowledged. M. R. funded by the Contract No. FIRB-2012-RBFR12PM1F from the Italian Ministry of Education, University and Research (MIUR).

*brandon.anderson@fysik.su.se
†kadrlica@fnal.gov
‡mdwood@slac.stanford.edu
§Permanent address: Naval Research Laboratory, Washington, DC 20375, USA.

[1] P. A. R. Ade *et al.* (Planck Collaboration), arXiv:1502.01589.
[2] G. Jungman, M. Kamionkowski, and K. Griest, Phys. Rep. **267**, 195 (1996).
[3] L. Bergstrom, Rep. Prog. Phys. **63**, 793 (2000).
[4] G. Bertone, D. Hooper, and J. Silk, Phys. Rep. **405**, 279 (2005).
[5] G. Steigman, B. Dasgupta, and J. F. Beacom, Phys. Rev. D **86**, 023506 (2012).
[6] M. Mateo, Annu. Rev. Astron. Astrophys. **36**, 435 (1998).
[7] A. W. McConnachie, Astron. J. **144**, 4 (2012).
[8] G. D. Martinez, Mon. Not. R. Astron. Soc. **451**, 2524 (2015).
[9] A. Geringer-Sameth, S. M. Koushiappas, and M. Walker, Astrophys. J. **801**, 74 (2014).
[10] M. Ackermann *et al.* (Fermi-LAT Collaboration), Phys. Rev. Lett. **107**, 241302 (2011).
[11] A. Geringer-Sameth and S. M. Koushiappas, Phys. Rev. Lett. **107**, 241303 (2011).
[12] M. N. Mazziotta, F. Loparco, F. de Palma, and N. Giglietto, Astropart. Phys. **37**, 26 (2012).
[13] M. Ackermann *et al.* (Fermi-LAT Collaboration), Phys. Rev. D **89**, 042001 (2014).
[14] A. Geringer-Sameth, S. M. Koushiappas, and M. G. Walker, Phys. Rev. D **91**, 083535 (2015).
[15] B. Anderson, J. Chiang, J. Cohen-Tanugi, J. Conrad, A. Drlica-Wagner, M. Llena Garde, and Stephan Zimmer (Fermi-LAT Collaboration), *Using Likelihood for Combined Data Set Analysis*, eConf C14102.1 (2014).
[16] T. Daylan, D. P. Finkbeiner, D. Hooper, T. Linden, S. K. N. Portillo *et al.*, arXiv:1402.6703.
[17] C. Gordon and O. Macias, Phys. Rev. D **88**, 083521 (2013).
[18] K. N. Abazajian, N. Canac, S. Horiuchi, and M. Kaplinghat, Phys. Rev. D **90**, 023526 (2014).
[19] F. Calore, I. Cholis, and C. Weniger, J. Cosmol. Astropart. Phys. 03 (2015) 038.
[20] W. Atwood *et al.* (Fermi-LAT Collaboration), *Pass 8: Toward the Full Realization of the Fermi-LAT Scientific Potential, Monterey, CA, 2013*, eConf C121028 (2013).
[21] F. Acero *et al.* (Fermi-LAT Collaboration), Astrophys. J. Suppl. Ser. **218**, 23 (2015).
[22] See Supplemental Material at http://link.aps.org/supplemental/10.1103/PhysRevLett.115.231301, for further information about the data analysis and preparation and a more detailed assessment of systematic uncertainties, which includes Refs. [23–33].
[23] M. Ackermann *et al.* (Fermi-LAT Collaboration), Astrophys. J. Suppl. Ser. **203**, 4 (2012).
[24] J. Bregeon *et al.* (Fermi-LAT Collaboration), *Fermi-LAT data reprocessed with updated calibration constants, Rome, Italy, 2013*, eConf C121028 (2013).
[25] S. K. Portillo and D. P. Finkbeiner, Astrophys. J. **796**, 54 (2014).
[26] J. Mattox, D. Bertsch, J. Chiang, B. Dingus, S. Digel *et al.*, Astrophys. J. **461**, 396 (1996).
[27] W. A. Rolke, A. M. Lopez, and J. Conrad, Nucl. Instrum. Methods Phys. Res., Sect. A **551**, 493 (2005).
[28] H. Jeffreys, Proc. R. Soc. A **186**, 453 (1946).
[29] A. Burkert, Astrophys. J. **447**, 25 (1995).
[30] F. de Palma, T. Brandt, G. Johannesson, and L. Tibaldo (Fermi-LAT Collaboration), *A Method for Exploring Systematics Due to Galactic Interstellar Emission Modeling: Application to the Fermi LAT SNR Catalog, Monterey, CA, 2013*, eConf C121028 (2013).

[31] E. Carlson, D. Hooper, and T. Linden, Phys. Rev. D **91**, 061302 (2015).
[32] L. E. Strigari, S. M. Koushiappas, J. S. Bullock, M. Kaplinghat, J. D. Simon, M. Geha, and B. Willman, Astrophys. J. **678**, 614 (2008).
[33] R. Essig, N. Sehgal, and L. E. Strigari, Phys. Rev. D **80**, 023506 (2009).
[34] M. Dall'Ora, G. Clementini, K. Kinemuchi, V. Ripepi, M. Marconi, L. Di Fabrizio, C. Greco, C. T. Rodgers, C. Kuehn, and H. A. Smith, Astrophys. J. **653**, L109 (2006).
[35] J. D. Simon and M. Geha, Astrophys. J. **670**, 313 (2007).
[36] M. G. Walker, M. Mateo, and E. W. Olszewski, Astron. J. **137**, 3100 (2009).
[37] R. R. Muñoz, P. M. Frinchaboy, S. R. Majewski, J. R. Kuhn, M.-Y. Chou, C. Palma, S. Tony Sohn, R. J. Patterson, and M. H. Siegel, Astrophys. J. **631**, L137 (2005).
[38] A. Koch, J. T. Kleyna, M. I. Wilkinson, E. K. Grebel, G. F. Gilmore, N. Wyn Evans, R. F. G. Wyse, and D. R. Harbeck, Astron. J. **134**, 566 (2007).
[39] J. D. Simon, M. Geha, Q. E. Minor, G. D. Martinez, E. N. Kirby *et al.*, Astrophys. J. **733**, 46 (2011).
[40] B. Willman, M. Geha, J. Strader, L. E. Strigari, J. D. Simon, E. Kirby, N. Ho, and A. Warres, Astron. J. **142**, 128 (2011).
[41] M. Mateo, E. W. Olszewski, and M. G. Walker, Astrophys. J. **675**, 201 (2008).
[42] M. G. Walker, in *Planets, Stars and Stellar Systems*, edited by T. D. Oswalt, I. S. McLean, H. E. Bond, L. M. French, P. Kalas, M. A. Barstow, G. Gilmore, W. C. Keel (Springer, Netherlands, 2013), Vol. 5, pp. 1039–1089.
[43] G. Battaglia, A. Helmi, and M. Breddels, New Astron. Rev. **57**, 52 (2013).
[44] L. E. Strigari, Phys. Rep. **531**, 1 (2013).
[45] M. G. Walker, M. Mateo, E. W. Olszewski, J. Penarrubia, N. Evans *et al.*, Astrophys. J. **704**, 1274 (2009).
[46] J. Wolf, G. D. Martinez, J. S. Bullock, M. Kaplinghat, M. Geha *et al.*, Mon. Not. R. Astron. Soc. **406**, 1220 (2010).
[47] G. D. Martinez, J. S. Bullock, M. Kaplinghat, L. E. Strigari, and R. Trotta, J. Cosmol. Astropart. Phys. 06 (2009) 014.
[48] J. F. Navarro, C. S. Frenk, and S. D. White, Astrophys. J. **490**, 493 (1997).
[49] M. Ackermann *et al.* (The Fermi LAT Collaboration), Astrophys. J. **799**, 86 (2014).
[50] http://fermi.gsfc.nasa.gov/ssc/data/analysis/software.
[51] http://fermi.gsfc.nasa.gov/ssc/data/access/lat/BackgroundModels.html.
[52] T. E. Jeltema and S. Profumo, J. Cosmol. Astropart. Phys. 11 (2008) 003.
[53] T. Sjöstrand, S. Mrenna, and P. Z. Skands, Comput. Phys. Commun. **178**, 852 (2008).
[54] Selected to have kinematically determined $J$ factors and avoid ROI overlap. The set is identical to that in Ackermann *et al.* [13].
[55] H. Chernoff, Ann. Math. Stat. **25**, 573 (1954).
[56] Results for all channels as well as bin-by-bin likelihood functions for each target are available in machine-readable format at http://www-glast.stanford.edu/pub_data/1048/.
[57] M. Ackermann *et al.* (Fermi-LAT Collaboration), Astrophys. J. **761**, 91 (2012).
[58] A. Abramowski *et al.* (H.E.S.S. Collaboration), Phys. Rev. Lett. **106**, 161301 (2011).
[59] J. Aleksić, S. Ansoldi, L. Antonelli, P. Antoranz, A. Babic *et al.* (MAGIC Collaboration), J. Cosmol. Astropart. Phys. 02 (2014) 008.
[60] K. N. Abazajian and J. P. Harding, J. Cosmol. Astropart. Phys. 01 (2012) 041.
[61] P. Agrawal, B. Batell, P. J. Fox, and R. Harnik, J. Cosmol. Astropart. Phys. 05 (2015) 011.
[62] T. Abbott *et al.* (DES Collaboration), arXiv:astro-ph/0510346.
[63] Z. Ivezic, J. Tyson, R. Allsman, J. Andrew, and R. Angel (LSST Collaboration), arXiv:0805.2366.